Author Manuscript

Author Manuscript

Author Manuscript

Author Manuscript

HHS Public Access

Author manuscript

Aging Cancer. Author manuscript; available in PMC 2023 June 01.

Published in final edited form as:

Aging Cancer. 2022 June ; 3(2): 116–129. doi:10.1002/aac2.12049.

Another Wrinkle with Age: Aged Collagen and Intra-peritoneal Metastasis of Ovarian Cancer

Elizabeth I. Harper[1,2,3], **Tyvette S. Hilliard**[1,2], **Emma F. Sheedy**[2], **Preston Carey**[2], **Paul Wilkinson**[2], **Michael D. Siroky**[1,2], **Jing Yang**[1,2], **Elizabeth Agadi**[1,2,3], **Annemarie K. Leonard**[1,2], **Ethan Low**[1,2], **Yueying Liu**[1,2], **Arya Biragyn**[4], **Christina M. Annunziata**[5], **M. Sharon Stack**[1,2,*]

[1]Department of Chemistry & Biochemistry, Notre Dame, IN

[2]Harper Cancer Research Institute, Notre Dame, IN

[3]Integrated Biomedical Sciences Graduate Program, University of Notre Dame, Notre Dame, IN

[4]National Institute on Aging, Bethesda, MD

[5]National Cancer Institute, Bethesda, MD

Abstract

Background: Age is the most significant risk factor for ovarian cancer (OvCa), the deadliest gynecologic malignancy. Metastasizing OvCa cells adhere to the omentum, a peritoneal structure rich in collagen, adipocytes, and immune cells. Ultrastructural changes in the omentum and the omental collagen matrix with aging have not been evaluated.

Aim: The aim of this study was to test the hypothesis that age-related changes in collagen in the ovarian tumor microenvironment promote OvCa metastatic success in the aged host.

Methods/Results: Young (3–6 months) and aged mice (20–23 months) were used to study the role of aging in metastatic success. Intra-peritoneal (IP) injection of ID8 *Trp53*$^{-/-}$ ovarian cancer cells showed enhanced IP dissemination in aged *vs* young mice. *In vitro* assays using purified collagen demonstrated reduced collagenolysis of aged fibers, as visualized using scanning electron microscopy (SEM) and quantified with a hydroxyproline release assay. Omental tumors in young and aged mice showed similar collagen deposition; however enhanced intra-tumoral collagen remodeling was seen in aged mice probed with a biotinylated collagen hybridizing peptide (CHP). In contrast, second harmonic generation (SHG) microscopy showed significant differences in collagen fiber structure and organization in omental tissue and SEM demonstrated enhanced omental fenestration in aged omenta. Combined SHG and Alexa Fluor-CHP microscopy *in vivo* demonstrated that peri-tumoral collagen was remodeled more extensively in young mice.

*To whom correspondence should be addressed: Dr. M. Sharon Stack, University of Notre Dame, A200D Harper Hall, 1234 N. Notre Dame Avenue, South Bend, IN 46617, Ph: 574-631-4100, Sharon.Stack.11@nd.edu.

Author Contribution Statement

All authors had full access to the data in the study and take responsibility for the integrity of the data and the accuracy of the data analysis. *Conceptualization,* E.I.H., T.S.H., A.B., C.M.A., M.S.S; *Methodology,* E.I.H., T.S.H., Y.L.; *Investigation,* E.I.H., E.F.S., P.C., P.W., M.D.S., J.Y., E.A., A.K.L., E.L.; *Formal Analysis,* E.I.H.; *Resources,* M.S.S.; *Writing- Original Draft,* E.I.H.; *Writing- Review & Editing,* T.S.H., M.S.S.; *Supervision,* M.S.S.*; Funding Acquisition,* E.I.H., A.B., C.M.A., M.S.S.

The authors have stated explicitly that there are no conflicts of interest in connection with this article.

Author Manuscript Author Manuscript Author Manuscript Author Manuscript

This collagen population represents truly aged host collagen, in contrast to intra-tumoral collagen that is newly synthesized, likely by cancer associated fibroblasts (CAFs).

Conclusions: Our results demonstrate that tumors in an aged host can grow with minimal collagen remodeling, while tumors in the young host must remodel peri-tumoral collagen to enable effective proliferation, providing a mechanism whereby age-induced ultrastructural changes in collagen and collagen-rich omenta establish a permissive pre-metastatic niche contributing to enhanced OvCa metastatic success in the aged host.

Graphical Abstract

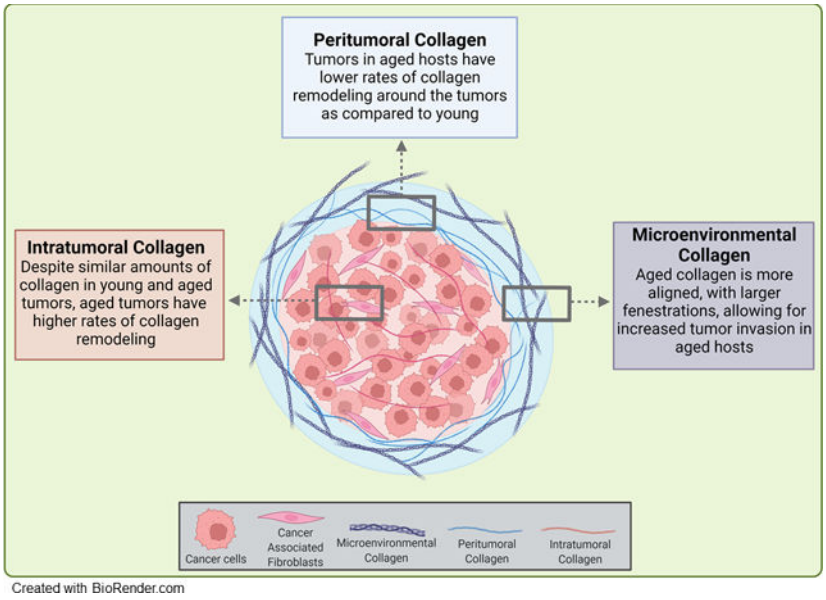

Age is a significant risk factor for ovarian cancer (OC) and pre-clinical models show enhanced metastatic success in aged (A) mice relative to young (Y). Intratumoral collagen remodeling was enhanced in A mice while peritumoral collagen was remodeled more extensively in Y mice. Age-associated changes in omental ultrastructure and collagen organization were observed in tumor naïve mice, suggesting the development of a permissive pre-metastatic niche contributing to enhanced metastatic success in the aged host.

Keywords

ovarian cancer; metastasis; aging; collagen; omentum

1. Introduction

Ovarian cancer (OvCa) is the deadliest gynecologic malignancy, with a five year survival rate below 50% [1]. Age is the most significant risk factor for OvCa, with a median age of 63 at diagnosis and median age of 70 for cancer-related deaths [1]. Epidemiological studies performed over three decades ago documented a disparity in cancer-related deaths between young and aged patients independent of treatment pathway [2]. Pre-clinical studies using aging murine models support these data, showing increased peritoneal tumor burden in aged

Author Manuscript Author Manuscript Author Manuscript Author Manuscript

mice relative to young in both C57Bl/6 and FVB backgrounds [3,4]; however, the molecular mechanisms by which aged individuals exhibit enhanced metastatic growth remains unclear.

OvCa metastasizes in a unique fashion where single cells or multi-cellular aggregates (MCAs) are exfoliated from the primary ovarian or fallopian tube tumor directly into the peritoneal cavity. Intra-peritoneal (IP) metastases are initiated by adhesion to sites in the peritoneal cavity such as the omentum and the parietal peritoneum. These sites are composed of a monolayer of mesothelial cells covering a collagen-rich extracellular matrix (ECM) [5,6]. Metastasizing OvCa cells initially target the omentum, a section of the peritoneum that folds between the parietal peritoneum and the abdominal organs [5]. This organ is rich in collagen, adipocytes, and immune cells [7,8] and acts as an abdominal filter to maintain homeostasis in the peritoneal cavity [9].

The sub-mesothelial matrix of the omentum is rich in collagen, the most abundant protein in the body. Collagen I (CI) is a fibrillar collagen, comprised of triple helical fibrils with a high content of proline, hydroxyproline, and glycine. It has previously been demonstrated that OvCa cells and MCAs bind preferentially to CI via the α2β1 and α3β1 integrins [10–12]. ECM organization both in normal physiological processes and in cancer is influenced by matrix metalloproteinase (MMP) activity. MMPs are a family of extracellular zinc-dependent enzymes including collagenases and gelatinases that function predominantly to remodel ECM proteins and to process other substrates [13–15]. While most MMP family members are secreted enzymes, a subclass are membrane-associated [14,16]. Previous studies have shown that the interstitial collagenase designated membrane-type 1 MMP (MT1-MMP, MMP-14) is abundantly overexpressed in OvCa [17–20]. While MT1-MMP is not expressed in normal ovarian epithelial cells, expression is acquired in OvCa cells, and is elevated in metastatic lesions compared to paired primary tumors from the same patient [21,22]. MT1-MMP activity, stimulated in part by integrin-mediated signaling via SRC kinases and EGR1 expression, functions early in metastasis to induce MCA formation and dissemination, and also acts to promote anchoring of metastatic lesions through peri-cellular collagenolysis of the sub-mesothelial matrix [21,22]. MT1-MMP cleavage of collagen triple helices catalyzes localized unwinding or denaturation of the collagen molecule, resulting in structural remodeling of tumor-associated collagen [17,23,24].

The clinical significance of collagen remodeling is highlighted by the ‘tumor associated collagen signature’ (TACS), a scoring system with diagnostic potential for many tumor types, including OvCa [25–28]. Based on tumor-associated changes in collagen ultrastructure, three signatures have been defined: density of collagen (TACS 1), alignment of collagen (TACS 2), and alignment of fibers in relation to tumor orientation (TACS 3), establishing a link between collagen ultrastructure and clinical prognosis [25–28]. The presence of OvCa cells also promotes fibrosis, or deposition of ECM proteins by cancer-associated fibroblasts (CAFs). Recent data show that ovarian fibrosis is increased with age and suggest that the fibrotic ovary represents a premetastatic niche [29,30]. Activated fibroblasts are characterized by expression of dipeptidyl-peptidase-4 (DPP4, also known as CD26), a transmembrane glycoprotein with serine exopeptidase activity [31]. Inhibition of DPP4 induces apoptosis in OvCa cell lines, suggesting its importance in OvCa progression [32]. This is further supported by data showing that clinical usage of metformin is correlated

Author Manuscript Author Manuscript Author Manuscript Author Manuscript

with a decrease in age-associated ovarian fibrosis and that *DPP4* is the most significantly downregulated gene in the ovaries of aged women in the metformin cohort [30].

Aging is known to dysregulate many cellular functions, and aging effects on collagen-rich organs have been best documented in studies of the skin which, like the omentum, is primarily composed of CI and collagen III (CIII) [33]. Aged skin has a higher CI/CIII ratio, but less overall collagen, as measured by hydroxyproline content, resulting in reduced elasticity and tensility of the tissue [33–35]. Another study found decreased CI by histological analysis in the dermis in patients over 40 years of age, with less overall collagen and decreased collagen bundle size [36]. It is also known that collagen fibers from aged skin are more aligned relative to collagen from younger adult skin [35,36]. Additionally, collagen produced by aged fibroblasts is less dense and more anisotropic, leaving more space in the dermis relative to collagen produced by young fibroblasts [37]. With a half-life of over a decade, CI acquires significant age-associated post-translational modifications [36]. These modifications include covalent crosslinks between molecules, produced either by a non-enzymatic glycation process that forms advanced glycation end products (AGEs) or enzymatically catalyzed by lysyl oxidase (LOX) [38,39]. These post-translational modifications can also impact collagen structure, reducing tissue elasticity and decreasing susceptibility to remodeling by MMPs [40,43]. As tumor cell interaction with omental collagen is a key event in OvCa metastasis [5–9], in the current study we evaluated the hypothesis that age-related changes in collagen in the ovarian tumor microenvironment promote OvCa metastatic success in the aged host.

2. Methods

Murine aging models:

Cohorts of C57Bl/6 or FVB/NJ (Jackson Labs) were aged to either 3–6 months (designated Young or Y; equivalent to women 20–30 years of age) or 20–23 months (designated Aged or A; equivalent to women 60–67 years of age) [44]. All animal procedures were carried out according to the regulations of the Institutional Animal Care and Use Committee at the University of Notre Dame.

Murine allograft models:

ID8 *Trp53*$^{-/-}$ cells, a C57Bl/6 syngeneic murine ovarian epithelial carcinoma cell line with a p53 null mutation, were generously provided by Dr. McNeish, Glasgow, UK, and were RFP-tagged as previously described [17]. The ID8 *Trp53*$^{-/-}$ cells were cultured in Dulbecco's Modified Eagle Medium (DMEM; Corning) containing 4% Fetal Bovine Serum (FBS; Gibco), 1% Penicillin/Streptomycin (Pen/Strep; Sigma), and 1% Insulin-transferrin-sodium selenite (ITS; Sigma). To compare tumor growth parameters in the omenta of young and aged mice, syngeneic ID8 *Trp53*$^{-/-}$ cells (10^7) were injected IP into young or aged hosts to generate metastases [3]. Mice were sacrificed by CO_2 anesthesia followed by cervical dislocation at 3 weeks post-injection for omental multiphoton microscopic analysis (described below) or 5.5 weeks post-injection for imaging and tumor harvest. Ascites was collected post-sacrifice and the volume recorded. The peritoneal cavity was opened for *in situ* imaging and omenta were dissected out for *ex vivo* imaging. All imaging was done

Author Manuscript Author Manuscript Author Manuscript Author Manuscript

using Bruker *In Vivo* Xtreme imaging system. Images were analyzed for RFP signal and quantified in ImageJ.

Cell lines:

Patient derived epithelial ovarian cancer cell lines OVCAR5 and OVCAR8 were obtained from American Type Culture Collection (ATCC). Cells were cultured in Dulbecco's Modified Eagle Medium (DMEM; Corning) containing 10% Fetal Bovine Serum (FBS; Gibco), 1% Penicillin/Streptomycin (Pen/Strep; Sigma), and 1% Non-Essential Amino Acids (NEAA; Corning).

Collagen purification:

To compare interaction of OvCa cells with young and aged collagen *in vitro*, collagen was isolated from mouse tails. Tails were harvested from young and aged mice and tail tendons were dissected as described [45]. Briefly, tails were rinsed in 70% ethanol, then tendons were removed by gripping the tip of the tail with forceps and twisting until the skin breaks and the tendons dissociate. Tail tendons were cut from the remaining tail structures and rinsed in PBS. The isolated collagen fibers were dissolved in 0.5M acetic acid at 4°C overnight, filtered through a 40μm cell strainer to remove blood vessels, then centrifuged (24,000g, 3 hr) to remove cellular debris. Purified collagen was then aliquoted, adjusted to neutral pH with NaOH, lyophilized, and stored at −20°C until use. Collagen was resuspended in 0.01N HCl then diluted in appropriate buffers for use in assays.

Adhesion assay:

To evaluate whether cells adhere differentially to young and aged CI, adhesion assays were performed. Young or aged CI (10μg/mL in coating buffer 0.1M $NaCO_3$, pH9.6) was added to each well of a 24-well plate in duplicate and incubated at 37°C for 2 hours, then rinsed with PBS and dried and stored at 4°C until use. OvCa cells (5×10^5) were added and incubated for 30 min (OVCAR5) or 45 min (OVCAR8) in serum-free medium (SFM), washed once with PBS, then fixed and stained with DiffQuik Three-step Stain Set (Thermoscientific) and imaged. Adhesion assays were repeated in triplicate and cells from five areas of each filter were enumerated. Data were evaluated using Student's t-test.

Proliferation assay:

To measure changes in growth of OvCa cells cultured on young or aged collagen, a proliferation assay was performed. A 96-well plate was coated with young or aged collagen (10 μg/mL per well) as described above in triplicate, incubated at 4°C overnight, then rinsed with PBS, dried and stored at 4°C until use. Cells were resuspended at 30,000 cells/mL, and 100ul were added to each well. After culturing in a CO_2 incubator at 37°C for 24 hours, proliferation was measured with the XTT Cell Proliferation Assay Kit (Cayman Chemical, #10010200). Assays were repeated in triplicate and data were evaluated using Student's t-test.

Author Manuscript Author Manuscript Author Manuscript Author Manuscript

Invasion assay:

To compare the ability of OvCa cells to penetrate young and aged collagen gels, invasion assays were performed. Invasion filters (8.0 μm, Corning, item 354578) were prepared with young or aged collagen gels (100μg in coating buffer 0.1M $NaCO_3$, pH9.6), dried overnight, and stored at 4°C until use. Cells (2.5×10^5) were added to the invasion filter and allowed to invade for 8h (OVCAR8) or 24h (OVCAR5). Filters were fixed with Diff-Quik Three-step Stain Set (Thermoscientific) and bottom of filters were imaged with Aperio ScanScope CS to identify invading cells. Invasion assays were conducted in triplicate and cells from five areas of each filter were enumerated. Significance was determined with Student's t-test.

Tail tendon proteolysis:

To assess whether collagen fibers obtained from tail tendons of young *vs* aged mice exhibit differential susceptibility to collagenolysis, the soluble collagenase matrix metalloproteinase-1 (MMP-1) was employed. Tail tendons were dissected from young and aged mice (n=9) as described above, minced into ~1mg pieces, and placed into individual wells of a 96 well plate. MMP-1 proenzyme (Enzo Life Sciences, ALX-200–418-C005) was activated with 10mM 4-aminophenylmercuric acetate (APMA) at 37°C for 2 hr. Tendons were then incubated with 100uM of activated MMP-1 in collagenase buffer (50mM Tris-HCl containing 200mM NaCl and 5mM $CaCl_2$, pH 7.0) for 16 hr and reactions were stopped with 0.5M EDTA. Supernatants were saved for hydroxyproline assay and tendons were processed for scanning electron microscopic (SEM) imaging as described below. To quantify collagenolysis, harvested supernatant was subjected to hydroxyproline analysis using a colorimetric assay (Sigma, #MAK008–1KT). Equal amounts of supernatant and concentrated hydrochloric acid were added to polypropylene tubes and heated at 120°C for 3 hours. Samples were centrifuged at 10,000g for 3 minutes, and 150uL of supernatant was added to a 96 well plate with standards provided by the manufacturer and dried in 60°C oven. Reagents were prepared according to manufacturer's instructions. Chloramine T/Oxidation Buffer Mixture (100μl) was added to each well and incubated at room temperature for 5 minutes before addition of the diluted 4-(Dimethylamino)-benzaldehyde (DMAB) Reagent (100μl) to each well. The plate was incubated for 90 minutes at 60°C, then absorbance was measured at 560nm and compared to standard curve to determine amount of enzymatic cleavage.

Scanning Electron Microscopy (SEM) Imaging and Analysis:

Tail tendons from C57Bl/6 mice (n=9) following enzymatic digestion or omenta from young and aged tumor-naive FVB mice (n=5) were incubated overnight at 4°C in pre-fixative solution (2% glutaraldehyde, 2% paraformaldehyde in 0.1M Cacodylate buffer, pH 7.3), then fixed with 1% OsO_4 and dehydrated with ascending amounts of EtOH as described [46]. Samples were dried in a critical point dryer (Tousimis 931), then mounted on stubs with carbon stickers, silver painted and sputter-coated with iridium at a thickness of 5nm. Samples were imaged on a FESEM: Magellan 400 (FEI). Images of tendons with and without MMP-1 treatment were examined for differences in fiber structure. For omenta, after thresholding and despeckling, fenestration area percentage and size were performed on the images in ImageJ using the analyze particles function.

Author Manuscript Author Manuscript Author Manuscript Author Manuscript

Trichrome analysis:

To compare collagen content in young and aged C57Bl/6 omental tumors a trichrome analysis was performed. Tumor bearing omenta from young (n=15) and aged mice (n=13) [3] were fixed with 10% formalin, then paraffin embedded and sectioned (5μm). Sections were baked at 65°C for 1 hr and de-paraffinized by xylene then rehydrated and stained with a trichrome stain kit (Abcam). Briefly, slides were incubated in Bouin's fluid overnight, washed with water, then stained with Weigert's Iron Hematoxylin for 12 minutes. Slides were washed with water then stained with Biebrich Scarlett/Acid Fuschin solution for 10 minutes, then washed with water. Slides were then differentiated in phosphomolybdic/phosphotungstic acid for 15 minutes, changing to fresh solution halfway through. Lastly, slides were stained with aniline blue for 10 minutes, washed with water, differentiated in 1% acetic acid before dehydration in ascending concentrations of ethanol followed by xylene, and slides were mounted with Cytoseal XYL. Slides were imaged with Aperio ScanScope CS and analyzed with ImageScope software.

Histological analysis with collagen hybridizing peptide biotin conjugate (B-CHP):

To compare collagen remodeling in omental tumors in young or aged mice, a histological analysis with B-CHP was done. Tumor bearing omenta from young and aged mice (n=13) [3] were fixed with 10% formalin, then paraffin embedded and sectioned (5μm). Sections were de-paraffinized by xylene and were rehydrated in decreasing amounts of ethanol. Endogenous peroxidases were blocked with 3% H_2O_2. Slides were blocked with avidin/biotin blocking kit (Vector Laboratories, SP-2001), then blocked for 1 hour with 3% BSA in Tris buffered solution (TBS). Collagen hybridizing peptide biotin conjugate (B-CHP [47], 3Helix, BIO300) was heated at 80°C for 5 minutes, cooled on ice for 30 seconds, diluted to 0.5μM in PBS, added to slides and incubated at 4°C overnight. Slides were washed with PBS and treated with Vectastain ABC kit (HRP) (Vector Laboratories) according to manufacturer specifications, developed with 3,3-diaminobenzene and counterstained with hematoxylin. Tissues were dehydrated in increasing concentrations of ethanol followed by xylene and mounted with Cytoseal XYL. Slides were imaged with Aperio ScanScope CS and analyzed with ImageScope software.

Immunohistochemical Analysis:

Tumor bearing omenta from young and aged mice (n=13) [3] were fixed with 10% formalin, then paraffin embedded and sectioned (5μm). Sections were de-paraffinized by xylene and were rehydrated in decreasing concentrations of ethanol. Antigen retrieval was done with 10mM sodium citrate, pH 6.0 (SMA, AGE antibodies) or Tris-EDTA buffer (10mM Tris, 1mM EDTA, 0.05% Tween 20, pH 9.0; DPP4 antibody). Endogenous peroxidases were blocked with 3% H_2O_2. Slides were blocked in horse serum, then incubated overnight at 4°C with an anti-AGE antibody (Abcam, ab23722, 1:10,000), an anti-SMA antibody (Abcam, ab5694, 1:1000), or anti-DPP4 antibody (Abcam, ab187048, 1:20,000) diluted in horse serum. All antibodies were then incubated with ImmPRESS HRP Horse Anti-Rabbit IgG (Vector Labs MP-7401) according to manufacturer's specifications, developed with 3,3-diaminobenzene and counterstained with hematoxylin. Tissues were dehydrated in

Author Manuscript Author Manuscript Author Manuscript Author Manuscript

increasing concentrations of ethanol followed by xylene and mounted with Cytoseal XYL. Slides were imaged with Aperio ScanScope CS and analyzed with ImageScope software.

Second harmonic generation (SHG) imaging and analysis of tumor-naïve omenta:

To visualize of collagen in the omenta of young and aged mice, SHG imaging was used. Young and aged tumor-naïve mice were sacrificed and omenta were harvested, cleaned with PBS, and placed onto 22×50 coverslips for imaging. Tissues were imaged on an Olympus FV1000 2-photon confocal microscope with XPLN 25X water objective. Organs were imaged in 3D with 1μm steps with the 860 laser with RXD1 emission filter. Anisotropic analysis was performed on the images with the FibrilTool plugin in ImageJ as described [48]. Total collagen and signal intensity were measured in ImageJ with the analyze particles function to measure area and raw integrated density, respectively.

SHG imaging and analysis of tumor-bearing omenta:

To visualize peri-tumoral collagen remodeling in omental metastases growing in young or aged mice, SHG was used in conjunction with 2-photon excitation fluorescence microscopy. Young and aged mice (n=5) were injected with RFP-tagged ID8 *Trp53*$^{-/-}$ cells (10^7) and tumors were allowed to develop for 3 weeks. B-CHP was prepared by heating peptide for 5 minutes at 80°C, then incubating with Alexa Fluor 647 conjugated to streptavidin for final concentrations of 40mM (B-CHP) and 10mM (Streptavidin-Alexa Fluor 647) in PBS. The CHP-Biotin:Alexa Fluor 647-Streptavidin mixture was then injected I.P. into tumor bearing and control mice for 3 hours before sacrifice. Omenta were dissected then imaged on Olympus FV1000 2-photon microscope with XPLN 25X water objective. Organs were imaged in 3D with 1μm steps with the 860 laser with RXD1 emission filter (SHG-Collagen), RXD3 emission filter (RFP-tagged OvCa Cells), and RXD4 emission filter (Alexa Fluor 647-tagged B-CHP). Amount of B-CHP was measured in ImageJ with the Analyze Particles function to measure area in the RXD4 channel.

Western blot analysis:

Western blotting was used to compare AGE content of young *vs* aged collagen, and MT1-MMP content in OVCAR5 *vs* OVCAR8 cells. Collagen was isolated as described above; cells were lysed with mRIPA lysis buffer (1% Triton X-100, 50 mM Tris, pH 7.5, 150mM NaCl, 5mM EDTA, 0.1% SDS, 20mM NaF, 10mM $Na_2P_2O_7$) supplemented with protease inhibitor mixture (Roche Applied Science). Protein content was measured by DC Protein Assay Kit (BioRad). Collagen samples (15ug) or cell lysates (20ug) were electrophoresed on a 9% SDS-PAGE gel and transferred to Immobilon-P PVDF membrane (Millipore) using a Trans-Blot Semi Dry transfer cell (BioRad). Membranes were blocked in 3% BSA for one hour at room temperature then incubated for 48 hrs at 4°C with anti-AGE antibody (Abcam, ab23722, 1:500) or anti-MT1-MMP antibody (Abcam, ab51074, 1:2000) diluted in 3% BSA in TBST buffer. Proteins were detected with HRP-conjugated goat anti-rabbit IgG (1:4000, Sigma-Aldrich). Blots were developed with SuperSignal West Dura extended duration substrate (Thermo Fisher Scientific) and detected using an ImageQuant LAS 4000 imager. MT1-MMP blots were stripped and reblotted with anti-β-actin-peroxidase antibody (A3854, Sigma; 10:100,000). Band intensities were quantified by densitometric analysis

Author Manuscript Author Manuscript Author Manuscript Author Manuscript

using ImageJ and presented as a ratio of MT1-MMP intensity normalized to β-actin loading control intensity.

Statistical Analysis:

Statistical significance is defined as $p<0.05$ as determined by Student's t-test. Error bars represent standard error of mean.

3. Results

3.1 Host age, tumor growth, and differential collagen invasion and remodeling

To examine the impact of host age on peritoneal dissemination, young and aged C57Bl/6 mice were injected IP with RFP-tagged ID8 *Trp53*$^{-/-}$ (10^7) and were sacrificed at 5.5 weeks to evaluate tumor burden *in situ* [Figure 1A,C] or in *ex vivo* omenta [Figure 1B,D]. Overall, enhanced tumor burden was observed in aged mice relative to young [Figure 1A–D] [3]. Ascites volume was also significantly greater in aged mice [Figure 1E]. A variety of *in vitro* functional assays were then used to model tumor cell interactions with the sub-mesothelial matrix that occur following tumor-initiated mesothelial cell retraction and exposure of the sub-mesothelial CI-rich matrix to which metastasizing OvCa cells avidly adhere, invade and proliferate to anchor secondary lesions [5,6]. Neither OvCa cell adhesion to nor proliferation on CI-coated surfaces were impacted by age of the host from which CI was purified [Figure S1A–B]. However, OVCAR5 cells exhibited significantly enhanced invasion through aged collagen gels relative to young collagen gels [Figure 2A]. Significant differences were not observed for OVCAR8 cells [Figure 2B] that express high endogenous levels of collagenolytic matrix metalloproteinases [Figure S2]. To further examine the impact of host age on collagenolysis, tail tendons isolated from young and aged mice were incubated with MMP-1 and the CI fibers were analyzed by SEM. Examination of CI from young hosts shows detachment of individual fibers from the main tendon, exposing internal fibers and thereby enabling penetration of the protease into the tendon [Figure 2D]. In contrast, in tendons from aged hosts, only the surface fibers were disrupted. The surface fibers are heavily digested but remain attached to the tendon, prohibiting further penetration of the tissue [Figure 2D], similar to results previously reported [41]. This is confirmed by analysis of hydroxyproline in the supernatants to quantify CI cleavage, showing enhanced hydroxyproline release from young tendon fibers relative to aged [Figure 2C]. Control experiments show that purified collagen from both young and aged hosts are susceptible to collagenolysis by MMP-1, generating the standard ¾ and ¼ degradation products [Figure 2E].

3.2 Intra-tumoral collagen remodeling is enhanced in tumors grown in aged hosts

To examine intra-tumoral collagen accumulation and integrity, fixed ID8 *Trp53*$^{-/-}$ omental tumors from young and aged host mice were examined using a variety of methods [3]. Initially, a trichrome stain was performed to measure the total amount of collagen present in the tumors. This analysis showed no significant difference in total intra-tumoral collagen quantity in young relative to aged tumors [Figure 3A]. Serial sections from the same tumors were affinity-stained with a biotin-tagged collagen hybridizing peptide (B-CHP) as described in Methods [47]. This reagent identifies only unfolded or remodeled

Author Manuscript Author Manuscript Author Manuscript Author Manuscript

collagen via hybridization of the B-CHP to denatured collagen chains, predominantly those generated following MMP-catalyzed cleavage, reforming a triple helical structure [47]. B-CHP staining demonstrated a significant increase in intra-tumoral collagen remodeling in aged tumors as compared to the young [Figure 3B]. Intra-tumoral collagen is likely newly synthesized, supported by the relative lack of advanced glycation end products (AGEs) in tumors from both young and aged hosts [Figure 3C] and by the similar content of smooth muscle actin (SMA) indicative of similar levels of cancer associated fibroblasts (CAFs) in both tumor cohorts [Figure 3D]. It is well documented that activated CAFs produce tumor-associated collagen [49]. DPP4 is a marker for activated fibrotic CAFS [50], and immunohistochemical analysis of DPP4 showed presence of activated CAFs in both cohorts [Figure 3E]. As aged tumors are larger than young [Figure 1], increased collagen remodeling may represent an increased need for ECM organization to support tumor growth.

3.3 Aging effects on peri-tumoral collagen in the host intra-peritoneal microenvironment

As potential aging-related alterations in CI ultrastructure have not been evaluated in the peritoneal microenvironment, SHG microscopy was used to image CI in tumor-naïve omental tissue directly without fixation or decellularization. SHG analysis showed significant differences in fiber structure and orientation, with long linear fibers (arrows) and thicker banding of CI fibers (arrowheads) in the aged tissues that are not present in the young [Figure 4A,B]. This contributes to the significantly enhanced anisotropy, or fiber alignment, in the aged omental CI relative to young [Figure 4C]. Area percentage analysis showed more collagen and an overall stronger SHG signal in aged omenta relative to young [Figure 4D,E].

Tumor-bearing young and aged mice were then used to evaluate peri-tumoral collagen remodeling *in vivo*. In these experiments, RFP-tagged omental tumors from young and aged mice were affinity-tagged with a CHP-B-streptavidin-Alexa Fluor 647 conjugate and imaged with 2-photon fluorescence microscopy in conjunction with SHG. In contrast to evaluation of intra-tumoral collagen remodeling, that showed increased remodeling in aged mice [Figure 2B], peri-tumoral collagen remodeling was enhanced in young mice relative to aged [Figure 5A,B]. To assess the presence of post-translational modifications accumulated with host collagen aging, AGE content was examined, as AGEs crosslink collagen and can block collagenolysis [41]. Western blot analysis of purified murine collagen showed an increase in AGE:collagen ratio [Figure 5C].

3.4 Ultrastructural analysis shows larger fenestrations in aged omenta relative to young

To evaluate further the ultrastructure of the omentum, tissues from tumor-naïve mice were examined by SEM. Notable differences were observed in omental fenestrations [Figure 6A,B], with significant increases in fenestration size and area observed in tissue from aged omenta [Figure 6C,D]. While a normal part of this tissue structure, the fenestrations in the aged omenta are larger than in the young [Figure 6C], and a fenestration area percentage analysis showed the fenestrations occupy a greater percentage of the omental area in the aged mice relative to young omenta [Figure 6D].

Author Manuscript Author Manuscript Author Manuscript Author Manuscript

4. Discussion

Age is a well-documented risk factor for OvCa incidence and negatively correlates with survival [1], [2]. These epidemiologic data are supported by pre-clinical models of aging and OvCa, showing enhanced metastatic success in aged mice relative to young using malignant cells derived from either the ovarian surface epithelium or the fallopian tube fimbriae in two distinct strains of mice [3,4]. Given the demonstrated importance of tumor cell interaction with interstitial collagen in OvCa IP metastasis [10–12,51], together with the widely studied analyses of age-related changes to dermal collagen [25,26,28,42], we hypothesized that age-related changes in omental collagen may contribute to the observed increase in OvCa metastatic success in aged mice. Our findings highlight the importance of independent consideration of “truly aged” peri-tumoral host collagen *vs* intra-tumoral collagen that is newly synthesized, even in aged hosts, by cells in the tumor microenvironment.

This concept is supported by SHG analysis of omental microenvironmental collagen in tumor-naïve mice, which showed a distinct difference in collagen ultrastructure in aged omenta as compared to young characterized by higher anisotropy, more collagen, and greater signal intensity in aged omenta. The increase in anisotropy has been shown in other cancer models to increase cancer cell motility [26,37]. Simply, the aligned fibers create a “highway” for cancer cells as compared to the “dirt road” meshwork of the young collagen. Aged omenta also have increased collagen content and collagen crosslinks that result in thicker banding and higher intensity of the SHG signal. Collagen fibers that are tightly bound together, as seen here in aged omenta, likely have fewer accessible sites for enzymatic cleavage [41,43]. Previous studies of metastatic microenvironments have shown that tumor cells remodel the ECM to generate TACS, including increased alignment of collagen fibers, increased collagen deposition, and increased crosslinking [26–28,43]. Indeed, ovarian cancer patients whose omental tumors exhibited enhanced tissue stiffness together with expression of a panel of ECM-associated genes and proteins, including *COL1A1*, were found to have poor overall survival [51]. This is consistent with recent findings linking ovarian cancer with fibrosis in aged ovaries [29,30]. Our results validate these concepts and demonstrate that the aged omental collagen microenvironment exhibits similar ultrastructural characteristics even in the absence of malignant cells, supporting the hypothesis that the aged omentum is primed for metastatic success.

In aged tumor-bearing mice, the peri-tumoral host collagen surrounding the tumor is not newly synthesized, and as such, represents the truly aged collagen of the microenvironment. Collagen has a half-life of several decades, so aged microenvironmental collagen can accumulate far more post-translational modifications relative to either young or newly synthesized collagen. This is supported by the increase in AGEs, observed in purified collagen from aged hosts, that crosslink fibrils and reduce susceptibility to remodeling [40–43]. In contrast, enhanced peri-tumor collagen remodeling *in vivo* was observed in young mice relative to aged using SHG/B-CHP analysis, consistent with collagen fibril degradation experiments showing that young collagen is more susceptible to collagenolysis. Moreover, these results also show that tumors in an aged host can grow with minimal collagen remodeling, while tumors in the young host must remodel the surrounding collagen to enable effective proliferation. While it is possible that this response is cell line specific,

Author Manuscript Author Manuscript Author Manuscript Author Manuscript

this finding is consistent with SEM data showing enhanced fenestration area in aged omenta, indicating that metastases in aged mice have sufficient space to initiate proliferation and expansion without the requirement for immediate matrix remodeling.

In summary, our results show significant age-associated changes in the ultrastructure of the peritoneal microenvironment in aged mice, characterized by altered collagen fiber organization and enhanced omental fenestration, that impact pericellular collagenolysis and tumor growth. As tumor cell interaction with omental collagen is a key event in OvCa metastasis [5–9,40–43,51], these data suggest that therapeutic strategies targeting structural changes in the aged ECM may be effective in aged patients. Future studies to evaluate cellular signal transduction networks activated by contact of tumor cells with young *vs* aged collagen and to elucidate distinct functional interplay of CAFs with the microenvironment of young *vs* aged hosts are also warranted.

Supplementary Material

Refer to Web version on PubMed Central for supplementary material.

ACKNOWLEDGEMENTS

This work was supported by National Institutes of Health grants F99 AG068527 (E.I.H.), KO1 CA218305 (T.S.H.), RO1 CA109545 (M.S.S.), and UO1 AG CA236797 (M.S.S., A.B., C.M.A) and the Samuel Waxman Cancer Research Foundation (M.S.S., A.B., C.M.A.). E.I.H. was previously a fellow of the Chemistry-Biochemistry-Biology Interface (CBBI) Program at the University of Notre Dame, supported by training grant T32 GM075762 from the National Institute of General Medical Sciences. The content is solely the responsibility of the authors and does not necessarily represent the official views of the National Institute of General Medical Sciences or the National Institutes of Health.

The *in vivo* imaging and scanning electron microscopy were conducted at the Notre Dame Integrated Imaging Facility. The second harmonic generation and 2-photon excitation fluorescence microscopy imaging were conducted at the Indiana University Imaging and Flow Cytometry Core Facility. Histological samples were imaged at the Harper Cancer Research Tissue Core Facility at Notre Dame. The lyophilization of collagen samples was conducted at the Center for Environmental Science and Technology (CEST) at the University of Notre Dame.

Data Availability Statement

Data sharing not applicable to this article as no datasets were generated or analyzed during the current study. The data that support the findings of this study are available from the corresponding author upon reasonable request.

References:

[1]. Howlader N et al. , “SEER Cancer Statistics Review, 1975–2014,” Natl. Cancer Inst, vol. Bethesda, MD, Apr. 2017, [Online]. Available: https://seer.cancer.gov/csr/1975_2014/

[2]. Yancik R, “Ovarian cancer: Age contrasts in incidence, histology, disease stage at diagnosis, and mortality,” Cancer, vol. 71, no. S2, pp. 517–523, doi: 10.1002/cncr.2820710205.

[3]. Loughran EA et al. , “Aging Increases Susceptibility to Ovarian Cancer Metastasis in Murine Allograft Models and Alters Immune Composition of Peritoneal Adipose Tissue,” Neoplasia, vol. 20, no. 6, pp. 621–631, Jun. 2018, doi: 10.1016/j.neo.2018.03.007. [PubMed: 29754071]

[4]. Cohen CA, Shea AA, Heffron CL, Schmelz EM, and Roberts PC, “The Parity-Associated Microenvironmental Niche in the Omental Fat Band Is Refractory to Ovarian Cancer Metastasis,” Cancer Prev. Res. (Phila. Pa.), vol. 6, no. 11, pp. 1182–1193, Nov. 2013, doi: 10.1158/1940-6207.CAPR-13-0227.

Author Manuscript Author Manuscript Author Manuscript Author Manuscript

[5]. Lengyel E, “Ovarian Cancer Development and Metastasis,” Am. J. Pathol, vol. 177, no. 3, pp. 1053–1064, Sep. 2010, doi: 10.2353/ajpath.2010.100105. [PubMed: 20651229]

[6]. Lengyel E et al. , “Epithelial ovarian cancer experimental models,” Oncogene, vol. 33, no. 28, pp. 3619–3633, Jul. 2014, doi: 10.1038/onc.2013.321. [PubMed: 23934194]

[7]. Nieman KM et al. , “Adipocytes promote ovarian cancer metastasis and provide energy for rapid tumor growth,” Nat. Med, vol. 17, no. 11, p. 1498, Nov. 2011, doi: 10.1038/nm.2492. [PubMed: 22037646]

[8]. Platell C, Cooper D, Papadimitriou JM, and Hall JC, “The omentum,” World J. Gastroenterol, vol. 6, no. 2, pp. 169–176, Apr. 2000, doi: 10.3748/wjg.v6.i2.169. [PubMed: 11819552]

[9]. Krist LFG et al. , “Cellular composition of milky spots in the human greater omentum: An immunochemical and ultrastructural study,” Anat. Rec, vol. 241, no. 2, pp. 163–174, Feb. 1995, doi: 10.1002/ar.1092410204. [PubMed: 7710133]

[10]. Moser TL, Pizzo SV, Bafetti LM, Fishman DA, and Stack MS, “Evidence for preferential adhesion of ovarian epithelial carcinoma cells to type I collagen mediated by the alpha2beta1 integrin,” Int. J. Cancer, vol. 67, no. 5, pp. 695–701, Sep. 1996, doi: 10.1002/(SICI)1097-0215(19960904)67:5<695::AID-IJC18>3.0.CO;2-4. [PubMed: 8782661]

[11]. Ellerbroek SM, Fishman DA, Kearns AS, Bafetti LM, and Stack MS, “Ovarian carcinoma regulation of matrix metalloproteinase-2 and membrane type 1 matrix metalloproteinase through beta1 integrin,” Cancer Res, vol. 59, no. 7, pp. 1635–1641, Apr. 1999. [PubMed: 10197640]

[12]. Burleson KM, Hansen LK, and Skubitz APN, “Ovarian carcinoma spheroids disaggregate on type I collagen and invade live human mesothelial cell monolayers,” Clin. Exp. Metastasis, vol. 21, no. 8, pp. 685–697, Jun. 2005, doi: 10.1007/s10585-004-5768-5.

[13]. Kessenbrock K, Plaks V, and Werb Z, “Matrix Metalloproteinases: Regulators of the Tumor Microenvironment,” Cell, vol. 141, no. 1, pp. 52–67, Apr. 2010, doi: 10.1016/j.cell.2010.03.015. [PubMed: 20371345]

[14]. Itoh Y, “Membrane-type matrix metalloproteinases: Their functions and regulations,” Matrix Biol. J. Int. Soc. Matrix Biol, vol. 44–46, pp. 207–223, Jul. 2015, doi: 10.1016/j.matbio.2015.03.004.

[15]. Rodríguez D, Morrison CJ, and Overall CM, “Matrix metalloproteinases: What do they not do? New substrates and biological roles identified by murine models and proteomics,” Biochim. Biophys. Acta BBA - Mol. Cell Res, vol. 1803, no. 1, pp. 39–54, Jan. 2010, doi: 10.1016/j.bbamcr.2009.09.015.

[16]. Jabłońska-Trypuć A, Matejczyk M, and Rosochacki S, “Matrix metalloproteinases (MMPs), the main extracellular matrix (ECM) enzymes in collagen degradation, as a target for anticancer drugs,” J. Enzyme Inhib. Med. Chem, vol. 31, no. sup1, pp. 177–183, Nov. 2016, doi: 10.3109/14756366.2016.1161620. [PubMed: 27028474]

[17]. Ellerbroek SM, Wu YI, Overall CM, and Stack MS, “Functional interplay between type I collagen and cell surface matrix metalloproteinase activity,” J. Biol. Chem, vol. 276, no. 27, pp. 24833–24842, Jul. 2001, doi: 10.1074/jbc.M005631200. [PubMed: 11331272]

[18]. Vos MC, van der Wurff AAM, van Kuppevelt TH, and Massuger LFAG, “The role of MMP-14 in ovarian cancer: a systematic review,” J. Ovarian Res, vol. 14, no. 1, p. 101, Dec. 2021, doi: 10.1186/s13048-021-00852-7. [PubMed: 34344453]

[19]. Afzal S et al. , “MT1-MMP and MMP-2 mRNA expression in human ovarian tumors: possible implications for the role of desmoplastic fibroblasts,” Hum. Pathol, vol. 29, no. 2, pp. 155–165, Feb. 1998, doi: 10.1016/s0046-8177(98)90226-x. [PubMed: 9490275]

[20]. Davidson B et al. , “High levels of MMP-2, MMP-9, MT1-MMP and TIMP-2 mRNA correlate with poor survival in ovarian carcinoma,” Clin. Exp. Metastasis, vol. 17, no. 10, pp. 799–808, 1999, doi: 10.1023/a:1006723011835. [PubMed: 11089877]

[21]. Barbolina MV, Adley BP, Ariztia EV, Liu Y, and Stack MS, “Microenvironmental regulation of membrane type 1 matrix metalloproteinase activity in ovarian carcinoma cells via collagen-induced EGR1 expression,” J. Biol. Chem, vol. 282, no. 7, pp. 4924–4931, Feb. 2007, doi: 10.1074/jbc.M608428200. [PubMed: 17158885]

[22]. Moss NM, Barbolina MV, Liu Y, Sun L, Munshi HG, and Stack MS, “Ovarian Cancer Cell Detachment and Multicellular Aggregate Formation Are Regulated by Membrane Type 1 Matrix

Author Manuscript Author Manuscript Author Manuscript Author Manuscript

Metalloproteinase: A Potential Role in I.p. Metastatic Dissemination," Cancer Res, vol. 69, no. 17, pp. 7121–7129, Sep. 2009, doi: 10.1158/0008-5472.CAN-08-4151. [PubMed: 19706774]

[23]. Manka SW et al. , "Structural insights into triple-helical collagen cleavage by matrix metalloproteinase 1," Proc. Natl. Acad. Sci, vol. 109, no. 31, pp. 12461–12466, Jul. 2012, doi: 10.1073/pnas.1204991109. [PubMed: 22761315]

[24]. Chung L et al. , "Collagenase unwinds triple-helical collagen prior to peptide bond hydrolysis," EMBO J, vol. 23, no. 15, pp. 3020–3030, Aug. 2004, doi: 10.1038/sj.emboj.7600318. [PubMed: 15257288]

[25]. Adur J et al. , "Second harmonic generation microscopy as a powerful diagnostic imaging modality for human ovarian cancer," J. Biophotonics, vol. 7, no. 1–2, pp. 37–48, 2014, doi: 10.1002/jbio.201200108. [PubMed: 23024013]

[26]. Conklin MW et al. , "Aligned Collagen Is a Prognostic Signature for Survival in Human Breast Carcinoma," Am. J. Pathol, vol. 178, no. 3, pp. 1221–1232, Mar. 2011, doi: 10.1016/j.ajpath.2010.11.076. [PubMed: 21356373]

[27]. Brett EA, Sauter MA, Machens H-G, and Duscher D, "Tumor-associated collagen signatures: pushing tumor boundaries," Cancer Metab, vol. 8, no. 1, p. 14, Dec. 2020, doi: 10.1186/s40170-020-00221-w. [PubMed: 32637098]

[28]. Cheon D-J et al. , "A collagen-remodeling gene signature regulated by TGF-β signaling is associated with metastasis and poor survival in serous ovarian cancer," Clin. Cancer Res. Off. J. Am. Assoc. Cancer Res, vol. 20, no. 3, pp. 711–723, Feb. 2014, doi: 10.1158/1078-0432.CCR-13-1256.

[29]. Landry DA, Vaishnav HT, and Vanderhyden BC, "The significance of ovarian fibrosis," Oncotarget, vol. 11, no. 47, pp. 4366–4370, Nov. 2020, doi: 10.18632/oncotarget.27822. [PubMed: 33315987]

[30]. McCloskey CW et al. , "Metformin Abrogates Age-Associated Ovarian Fibrosis," Clin. Cancer Res, vol. 26, no. 3, pp. 632–642, Feb. 2020, doi: 10.1158/1078-0432.CCR-19-0603. [PubMed: 31597663]

[31]. Borrelli MR et al. , "Pro-Fibrotic CD26-Positive Fibroblasts Are Present in Greater Abundance in Breast Capsule Tissue of Irradiated Breasts," Aesthet. Surg. J, vol. 40, no. 4, pp. 369–379, Mar. 2020, doi: 10.1093/asj/sjz109. [PubMed: 30972420]

[32]. Kosowska A et al. , "Sitagliptin Modulates the Response of Ovarian Cancer Cells to Chemotherapeutic Agents," Int. J. Mol. Sci, vol. 21, no. 23, p. E8976, Nov. 2020, doi: 10.3390/ijms21238976. [PubMed: 33256016]

[33]. Cheng W, Yan-hua R, Fang-gang N, and Guo-an Z, "The content and ratio of type I and III collagen in skin differ with age and injury," Afr. J. Biotechnol, vol. 10, no. 13, pp. 2524–2529, Jan. 2011.

[34]. Shin J-W et al. , "Molecular Mechanisms of Dermal Aging and Antiaging Approaches," Int. J. Mol. Sci, vol. 20, no. 9, p. E2126, Apr. 2019, doi: 10.3390/ijms20092126. [PubMed: 31036793]

[35]. Quan T and Fisher GJ, "Role of Age-Associated Alterations of the Dermal Extracellular Matrix Microenvironment in Human Skin Aging: A Mini-Review," Gerontology, vol. 61, no. 5, pp. 427–434, 2015, doi: 10.1159/000371708. [PubMed: 25660807]

[36]. Marcos-Garcés V et al. , "Age-related dermal collagen changes during development, maturation and ageing - a morphometric and comparative study," J. Anat, vol. 225, no. 1, pp. 98–108, Jul. 2014, doi: 10.1111/joa.12186. [PubMed: 24754576]

[37]. Kaur A et al. , "Remodeling of the Collagen Matrix in Aging Skin Promotes Melanoma Metastasis and Affects Immune Cell Motility," Cancer Discov, vol. 9, no. 1, pp. 64–81, Jan. 2019, doi: 10.1158/2159-8290.CD-18-0193. [PubMed: 30279173]

[38]. Gkogkolou P and Böhm M, "Advanced glycation end products," Dermatoendocrinol, vol. 4, no. 3, pp. 259–270, Jul. 2012, doi: 10.4161/derm.22028. [PubMed: 23467327]

[39]. Smith-Mungo LI and Kagan HM, "Lysyl oxidase: Properties, regulation and multiple functions in biology," Matrix Biol, vol. 16, no. 7, pp. 387–398, Feb. 1998, doi: 10.1016/S0945-053X(98)90012-9. [PubMed: 9524359]

Author Manuscript Author Manuscript Author Manuscript Author Manuscript

[40]. Goh KL et al. , “Ageing changes in the tensile properties of tendons: influence of collagen fibril volume fraction,” J. Biomech. Eng, vol. 130, no. 2, p. 021011, Apr. 2008, doi: 10.1115/1.2898732. [PubMed: 18412498]

[41]. Panwar P, Butler GS, Jamroz A, Azizi P, Overall CM, and Brömme D, “Aging-associated modifications of collagen affect its degradation by matrix metalloproteinases,” Matrix Biol, Jun. 2017, doi: 10.1016/j.matbio.2017.06.004.

[42]. Harper EI, Sheedy EF, and Stack MS, “With Great Age Comes Great Metastatic Ability: Ovarian Cancer and the Appeal of the Aging Peritoneal Microenvironment,” Cancers, vol. 10, no. 7, Jul. 2018, doi: 10.3390/cancers10070230.

[43]. Marino GE and Weeraratna AT, “A glitch in the matrix: Age-dependent changes in the extracellular matrix facilitate common sites of metastasis,” Aging Cancer, vol. 1, no. 1–4, pp. 19–29, Dec. 2020, doi: 10.1002/aac2.12013. [PubMed: 35694033]

[44]. Flurkey K, Currer JM, and Harrison DE, “Chapter 20 - Mouse Models in Aging Research,” in The Mouse in Biomedical Research (Second Edition), Fox JG, Davisson MT, Quimby FW, Barthold SW, Newcomer CE, and Smith AL, Eds. Burlington: Academic Press, 2007, pp. 637–672. doi: 10.1016/B978-012369454-6/50074-1.

[45]. Rajan N, Habermehl J, Coté M-F, Doillon CJ, and Mantovani D, “Preparation of ready-to-use, storable and reconstituted type I collagen from rat tail tendon for tissue engineering applications,” Nat. Protoc, vol. 1, no. 6, p. 2753, Dec. 2006, doi: 10.1038/nprot.2006.430. [PubMed: 17406532]

[46]. Leonard AK et al. , “Methods for the visualization and analysis of extracellular matrix protein structure and degradation,” Methods Cell Biol, vol. 143, pp. 79–95, 2018, doi: 10.1016/bs.mcb.2017.08.005. [PubMed: 29310793]

[47]. Hwang J et al. , “*In Situ* Imaging of Tissue Remodeling with Collagen Hybridizing Peptides,” ACS Nano, vol. 11, no. 10, pp. 9825–9835, Oct. 2017, doi: 10.1021/acsnano.7b03150. [PubMed: 28877431]

[48]. Boudaoud A et al. , “FibrilTool, an ImageJ plug-in to quantify fibrillar structures in raw microscopy images,” Nat. Protoc, vol. 9, no. 2, p. 457, Feb. 2014, doi: 10.1038/nprot.2014.024. [PubMed: 24481272]

[49]. Nissen NI, Karsdal M, and Willumsen N, “Collagens and Cancer associated fibroblasts in the reactive stroma and its relation to Cancer biology,” J. Exp. Clin. Cancer Res, vol. 38, no. 1, p. 115, Mar. 2019, doi: 10.1186/s13046-019-1110-6. [PubMed: 30841909]

[50]. Wang XM et al. , “The pro-fibrotic role of dipeptidyl peptidase 4 in carbon tetrachloride-induced experimental liver injury,” Immunol. Cell Biol, vol. 95, no. 5, pp. 443–453, May 2017, doi: 10.1038/icb.2016.116. [PubMed: 27899813]

[51]. Pearce OMT et al. , “Deconstruction of a Metastatic Tumor Microenvironment Reveals a Common Matrix Response in Human Cancers,” Cancer Discov, vol. 8, no. 3, pp. 304–319, Mar. 2018, doi: 10.1158/2159-8290.CD-17-0284. [PubMed: 29196464]

Author Manuscript Author Manuscript Author Manuscript Author Manuscript

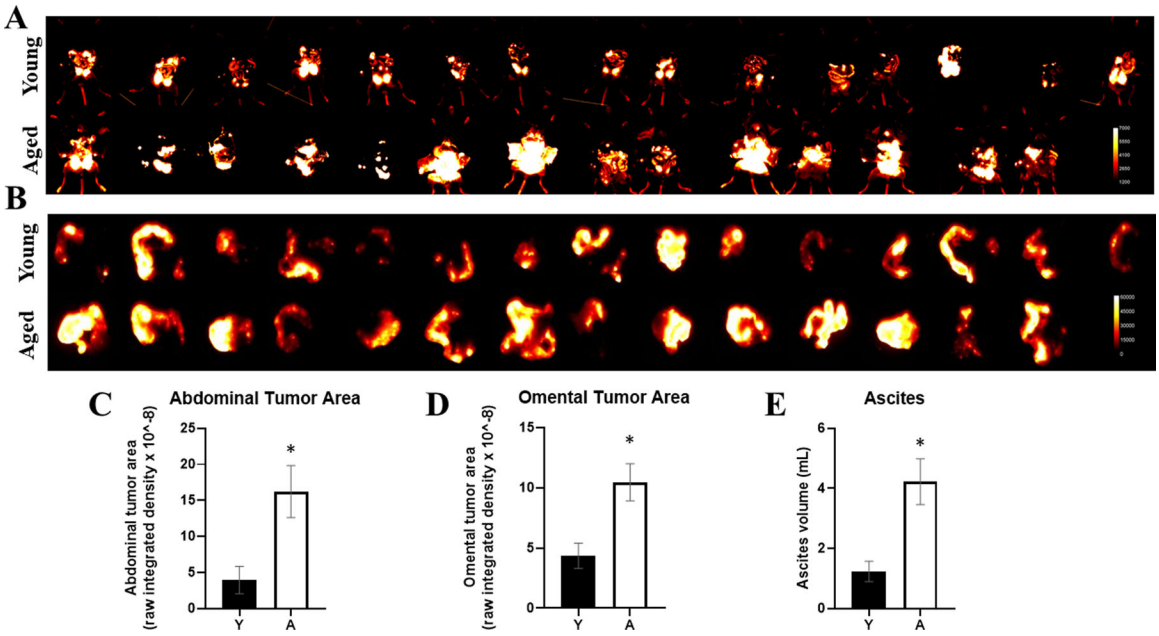

Figure 1. Enhanced growth of OvCa peritoneal metastases in aged mice.

C57Bl/6 mice at 3–6 months of age (Young; Y, n=15) or 20–23 months of age (Aged; A, n=14) were injected IP with RFP-tagged syngeneic ID8 *Trp53*$^{-/-}$ cells (10^7). Tumors were allowed to grow for 5.5 weeks, then mice were sacrificed and (A) the peritoneal cavity was exposed for *in situ* fluorescence imaging and (B) omenta were dissected and imaged *ex vivo*. RFP signal was quantified for (C) abdominal tumor burden (D) and omental tumor burden. (E) Ascites was collected post-sacrifice and the volume was measured. *p<0.005.

Author Manuscript Author Manuscript Author Manuscript Author Manuscript

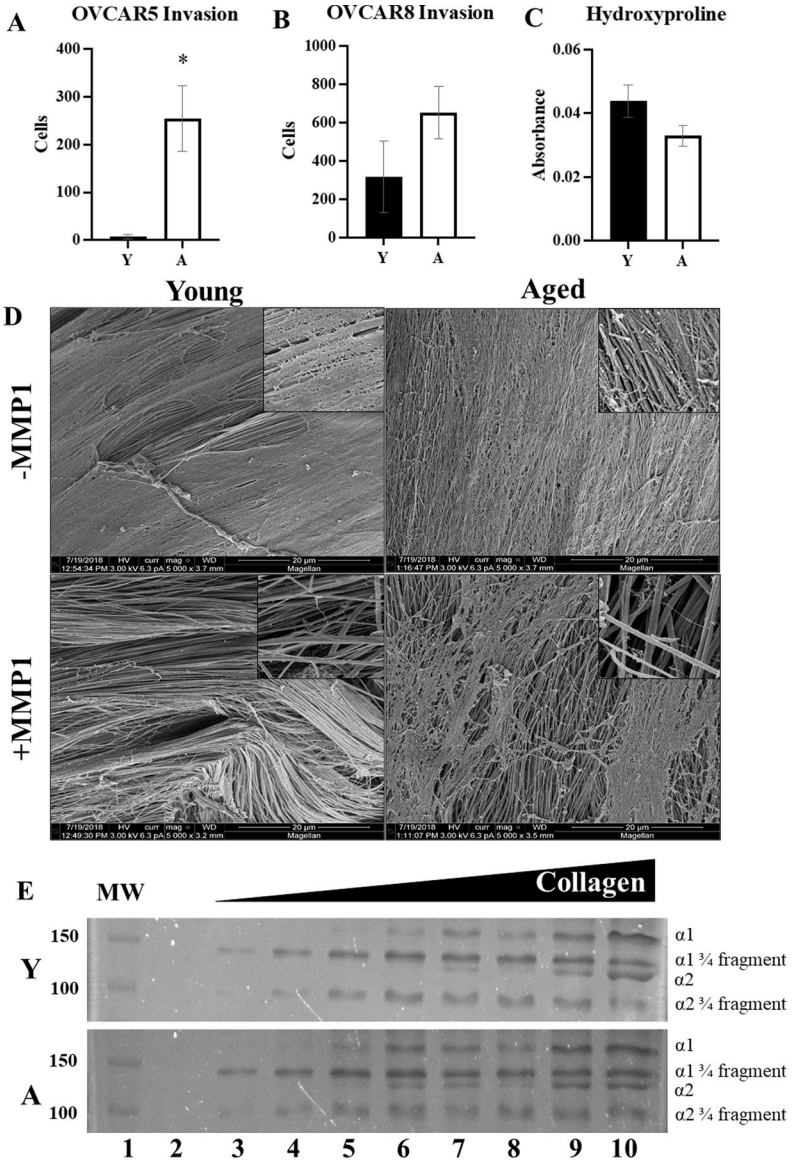

Figure 2. Analysis of collagen from young *vs* aged mice.

Collagen was isolated from young (Y) or aged (A) mice. (A,B) Invasion assays. Collagen was used to coat Boyden invasion chambers, followed by addition of the ovarian cancer cell lines (A) OVCAR5 or (B) OVCAR8 (2.5×10^5) to the wells for 8 or 24 hr, respectively. Invasion was quantified by enumerating cells on the bottom of the filter (n=3, p=0.02 OVCAR5, p=0.22 OVCAR8). (C) Degradation of collagen fibers. Whole tail tendons (n=9) from Y or A mice were incubated with pre-activated MMP-1 (100uM, 16 hr). The supernatant was collected and assayed for hydroxyproline content (p=0.09 as determined by Student's t-test). Error bars represent standard error of mean. (D) SEM of collagen degradation. Tendons from (C) were collected for scanning electron microscopy (5000x; inset 25,000x). (E) Cleavage products from (C) were electrophoresed on a 9% SDS-PAGE gel and stained with Coomassie to show the ¾ and ¼ fragments of the cleaved collagen. Lanes are: (1) molecular weight markers, (2) 0 μg collagen, (3) 4 μg collagen, (4) 6 μg

collagen, (5) 8 μg collagen, (6) 10 μg collagen, (7) 12.5μg collagen, (8) 15 μg collagen, 20μg collagen.

Author Manuscript Author Manuscript Author Manuscript Author Manuscript

Author Manuscript Author Manuscript Author Manuscript Author Manuscript

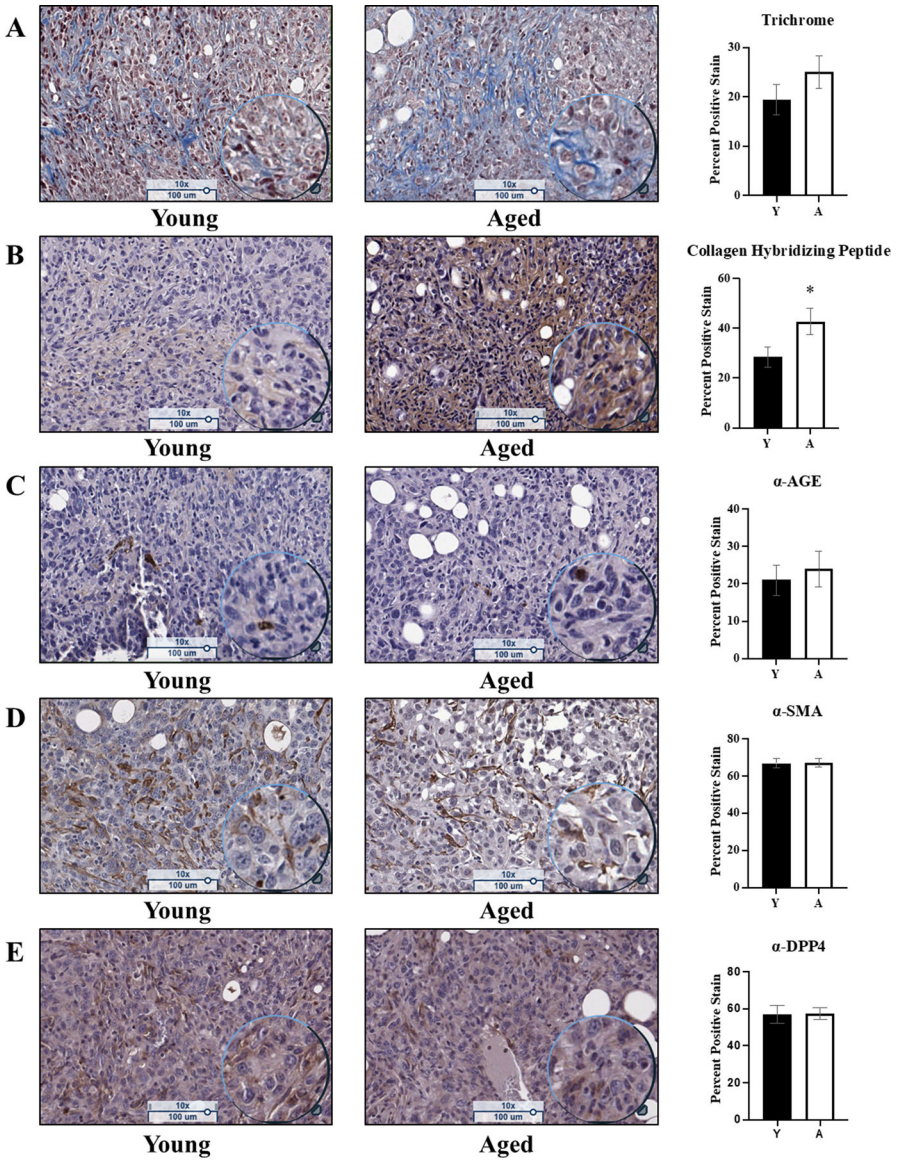

Figure 3. Histological and immunohistochemical analysis of omental tumors from young *vs* aged mice.

Omental tumors from young (n=15) and aged (n=13) C57Bl/6 mice were formalin fixed, paraffin embedded, and sectioned at 5μm width and stained with: (A) Trichrome, a marker for cell nuclei (purple), cell cytoplasm (pink), and collagen (blue), where the blue stain was quantified (p=0.23); (B) Affinity staining with the biotin-conjugated collagen hybridizing peptide, a marker for denatured collagen (brown) and counterstained with hematoxylin (cell nuclei; purple), where the brown signal was quantified (p=0.04); (C) Immunohistochemical analysis of advanced glycation end products (AGEs; brown) and counterstained with hematoxylin (cell nuclei; purple), where the positive brown stain was quantified (p=0.64); (D) Immunohistochemical analysis of smooth muscle actin (SMA; brown), a marker of cancer associated fibroblasts, and counterstained with hematoxylin (cell nuclei; purple), where the positive brown stain was quantified (p=0.89); (E) Immunohistochemical analysis of dipeptidyl-peptidase 4 (DPP4; brown), a marker of activated fibroblasts, and

Author Manuscript Author Manuscript Author Manuscript Author Manuscript

counterstained with hematoxylin (cell nuclei; purple), where the positive brown stain was quantified (p=0.53). Error bars represent standard error of mean and p-values were determined by Student's t-test.

Author Manuscript Author Manuscript Author Manuscript Author Manuscript

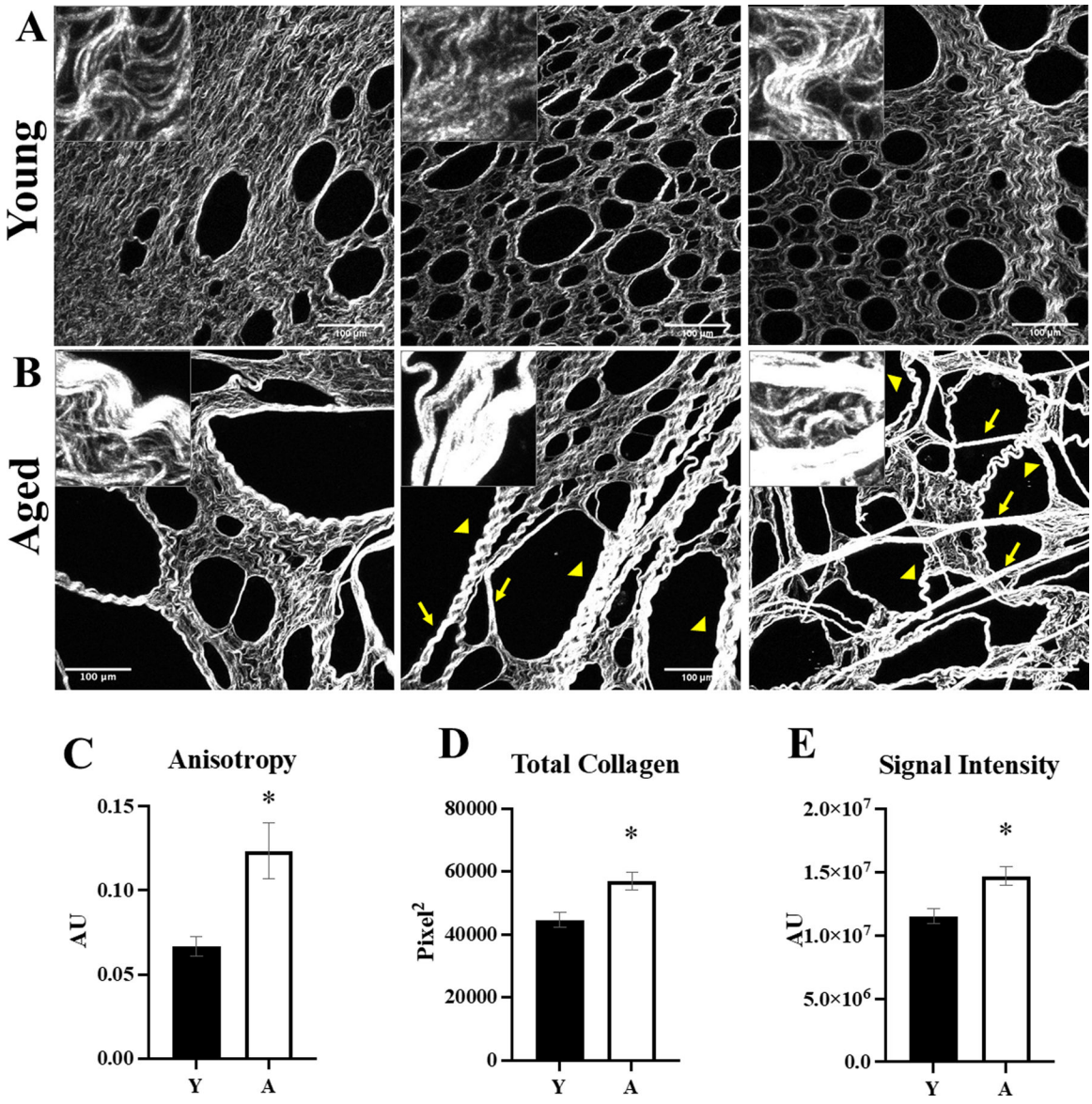

Figure 4. Second harmonic generation (SHG) microscopic analysis of tumor-naïve omenta from young and aged mice.

Omenta (n=5 per cohort) were obtained from (A) young (Y) or (B) aged (A) mice and the collagen was imaged with second harmonic generation (SHG) microscopy (25x; inset 100x). Aged omenta have longer, linear fibers (arrows) and thicker banding of fibers (arrowheads) relative to young omenta. Images were analyzed with ImageJ for (C) anisotropy, a measure of linearity (p=0.01); (D) total collagen (p=0.01); and (E) intensity of the SHG signal (p=0.01). Error bars represent standard error of mean and p-values were determined by Student's t-test.

Author Manuscript Author Manuscript Author Manuscript Author Manuscript

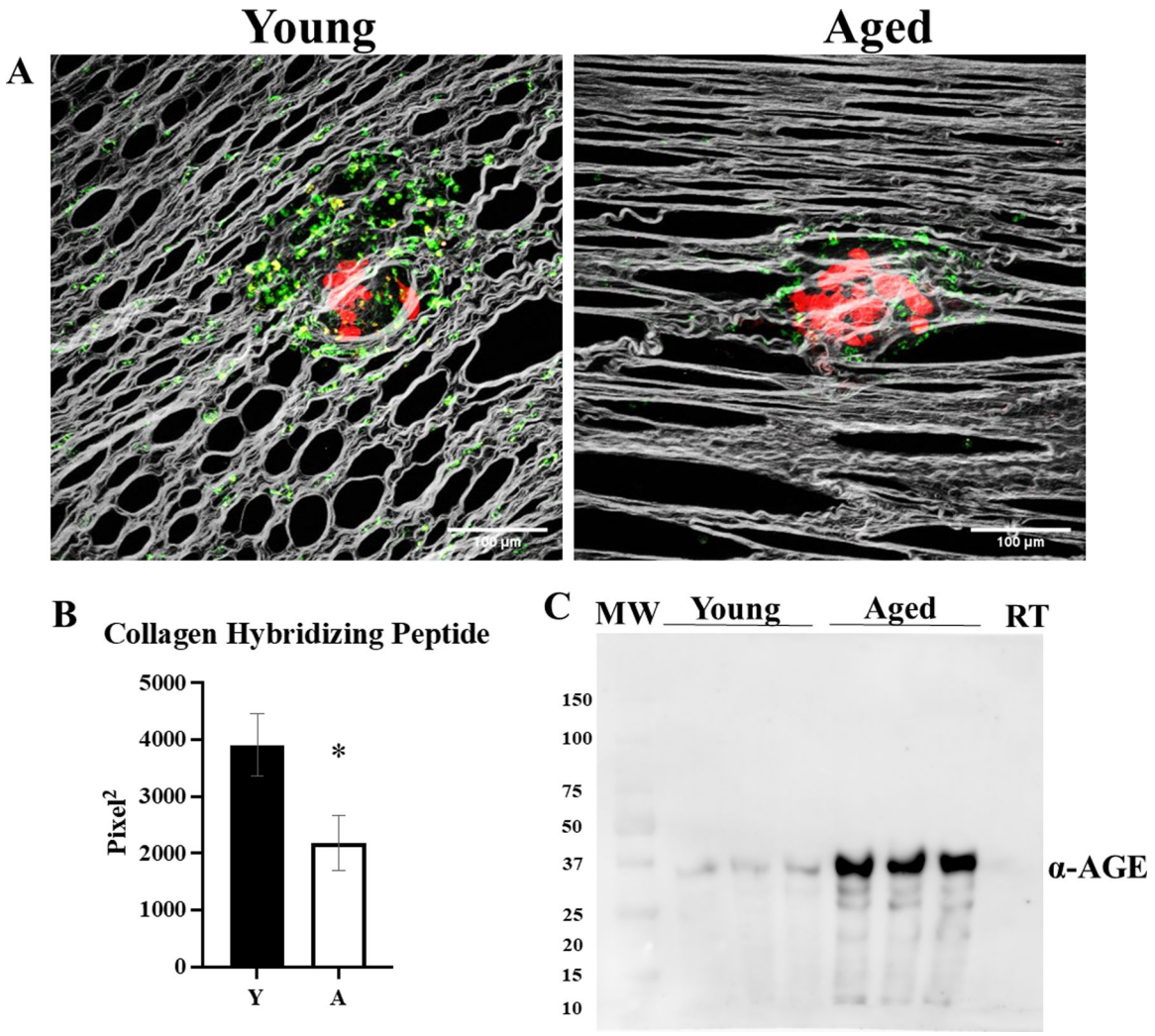

Figure 5. Visualization of peri-tumoral collagen remodeling in young and aged mice.

C57Bl/6 mice (n=5 per cohort) at 3–6 months of age (Young; Y) or 20–23 months of age (Aged; A) were injected IP with RFP-tagged syngeneic ID8*trp53*$^{-/-}$ cells (10^7). Tumors were allowed to grow for 3 weeks, then mice were injected with CHP-B:Streptavidin-Alexa Fluor 647 and sacrificed 3 hr post injection and omenta were imaged with SHG microscopy in conjunction with 2-photon excitation fluorescence microscopy to (A) visualize collagen (grey), tumor cells (red), and biotin conjugate of the collagen hybridizing peptide bound to Alexa Fluor 647 conjugated to streptavidin (pseudocolored green). (B) The images were analyzed for collagen hybridizing peptide signal (p=0.04). (C) Collagen isolated from young and aged mice, as well as commercially available rat tail (RT) collagen, was electrophoresed on a 9% SDS-PAGE gel, transferred to a PVDF membrane, probed with anti-AGE (1:500) and developed with a peroxidase-conjugated secondary antibody (anti-rabbit, 1:4000) and ECL detection. Error bars represent standard error of mean and p-values were determined by Student's t-test.

Author Manuscript Author Manuscript Author Manuscript Author Manuscript

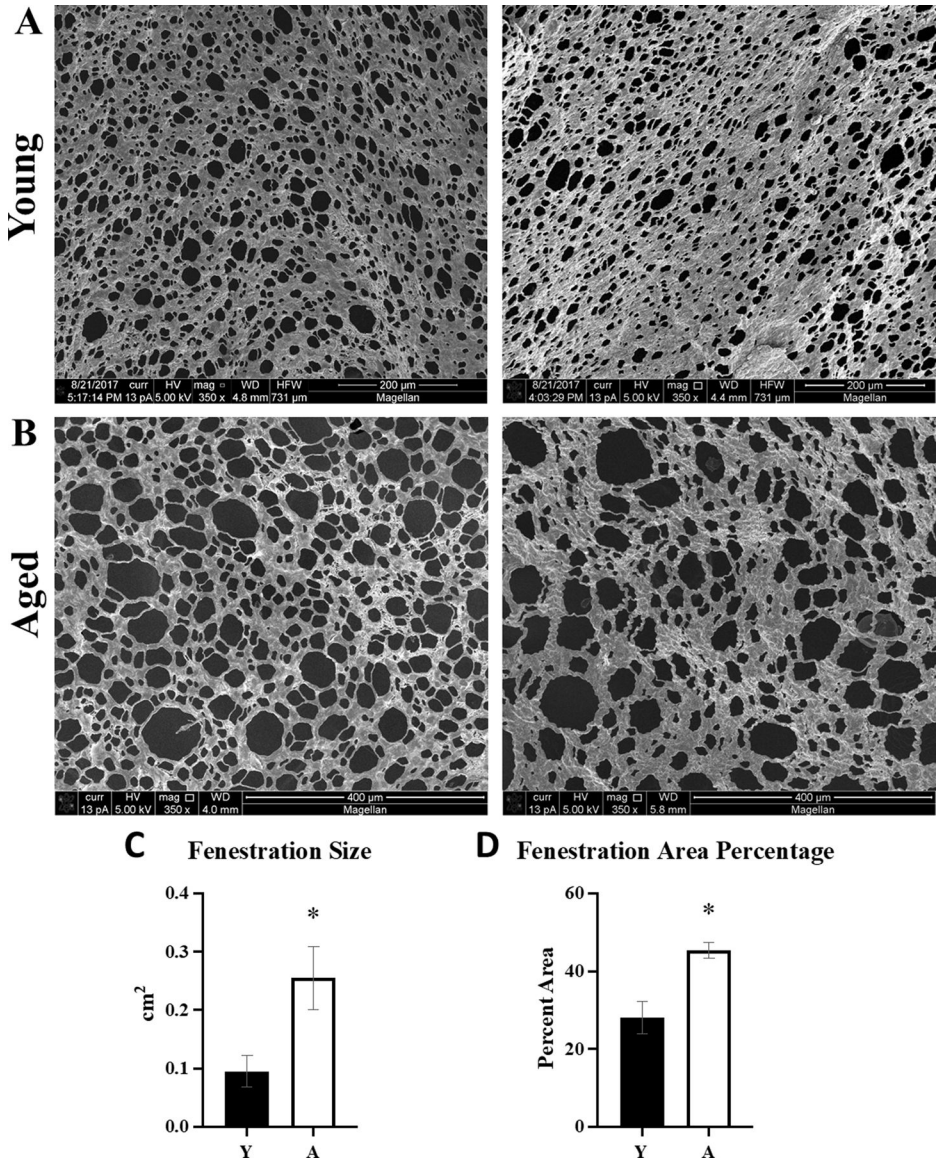

Figure 6. Analysis of omental fenestration in young *vs* aged mice.

Tumor-naive omenta (n=5) were obtained from (A) young (Y) or (B) aged (A) FVB/NJ mice and the collagen was imaged with SEM. Images were analyzed with ImageJ for (C) size of the fenestrations in the aged tissue as compared to young (p=0.03), and (D) overall area of the tissue represented by the fenestrations in aged compared to young (p=0.005). Error bars represent standard error of mean and p-values were determined by Student's t-test.